Pharm Res (2012) 29:2777–2791
DOI 10.1007/s11095-011-0655-7

RESEARCH PAPER

Stabilization of a Supersaturated Solution of Mefenamic Acid from a Solid Dispersion with EUDRAGIT® EPO

Taro Kojima • Kenjirou Higashi • Toyofumi Suzuki • Kazuo Tomono • Kunikazu Moribe • Keiji Yamamoto

Received: 13 April 2011 / Accepted: 13 December 2011 / Published online: 5 January 2012

ABSTRACT

Purpose The stabilization mechanism of a supersaturated solution of mefenamic acid (MFA) from a solid dispersion with EUDRAGIT® EPO (EPO) was investigated.

Methods The solid dispersions were prepared by cryogenic grinding method. Powder X-ray diffractometry, *in vitro* dissolution test, *in vivo* oral absorption study, infrared spectroscopy, and solid- and solution-state NMR spectroscopies were used to characterize the solid dispersions.

Results Dissolution tests in acetate buffer (pH 5.5) revealed that solid dispersion showed > 200-fold higher concentration of MFA. Supersaturated solution was stable over 1 month and exhibited improved oral bioavailability of MFA in rats, with a 7.8-fold higher area under the plasma concentration-*versus*-time curve. Solid-state ^{1}H spin–lattice relaxation time (T_1) measurement showed that MFA was almost monomolecularly dispersed in the EPO polymer matrix. Intermolecular interaction between MFA and EPO was indicated by solid-state infrared and ^{13}C-T_1 measurements. Solution-state ^{1}H-NMR measurement demonstrated that MFA existed in monomolecular state in supersaturated solution. ^{1}H-T_1 and difference nuclear Overhauser effect measurements indicated that cross relaxation occurred between MFA and EPO due to the small distance between them.

Conclusions The formation and high stability of the supersaturated solution were attributable to the specifically formed intermolecular interactions between MFA and EPO.

KEY WORDS solid dispersion · supersaturation · NMR · oral bioavailability · EUDRAGIT® EPO

INTRODUCTION

In recent years, progress in combinatorial chemistry and high-throughput screening has enabled the pharmaceutical industry to synthesize and evaluate an enormous number of compounds in a short time. This has resulted in an increase in new drug candidates with intense pharmacological activity. However, this emphasis on pharmacological activity has resulted in the creation of complex-structured compounds with high molecular weight (1). These compounds exhibit much lower bioavailability than expected from their potential druggability because of poor water solubility and permeability. The United States Food and Drug Administration (FDA) has proposed a biopharmaceutical classification system (BCS) that categorizes drugs into 4 classes based on their permeability and solubility (2). Drugs showing high permeability and low water solubility have been classified into class II. Although these drugs have advantageous membrane permeability, they cannot act effectively because the dissolution process is a limiting factor for drug absorption. Therefore, improving the solubility of poorly water-soluble drugs is one of the most important tasks for enhancing the absorption of class II drugs, and various approaches have been investigated, such as cocrystal formation (3), inclusion complex formation with cyclodextrin (4,5), encapsulation of drugs into emulsion (6), and nanoparticle formation to increase surface area (7,8).

Amorphization of crystalline drugs is one of the most frequently used methods for improving water solubility (9). The arrangement of drug molecules in the amorphous state is disordered while those in the crystalline state are regularly arrayed. This results in molecules in the amorphous state

Electronic supplementary material The online version of this article (doi:10.1007/s11095-011-0655-7) contains supplementary material, which is available to authorized users.

T. Kojima • K. Higashi • T. Suzuki • K. Tomono • K. Moribe • K. Yamamoto (✉)
Chiba University
Chiba, Japan
e-mail: yamamotk@p.chiba-u.ac.jp

that possess higher energy than molecules in the crystalline state (10). When amorphous drugs are dispersed into water, a supersaturated solution that exceeds the solubility of the crystalline drug at the same temperature can be obtained. However, it is thermodynamically difficult to prepare a stable amorphous drug by itself. Consequently, solid dispersions, where the drug molecules are dispersed monomolecularly into a carrier matrix, have been studied (11,12). Many water-soluble polymers can be used as carriers that accelerate amorphization of crystalline drugs and stabilize amorphous drugs in the solid state (13–15). These polymers can also inhibit recrystallization of drugs from supersaturated solution, resulting in stabilization of the supersaturated state in solution (16). For these reasons, solid dispersions are expected to improve *in vitro* dissolution and *in vivo* oral bioavailability of poorly water-soluble drugs (17). However, drug recrystallization may occur even in solid dispersions due to mechanical stress, heat, and humidity. There are few examples of solid dispersions of pharmaceutical products that offer long storage stability in the amorphous state over several years (18). Furthermore, supersaturated solutions obtained from solid dispersions are still thermodynamically unstable, and drug recrystallization in water must be induced gradually. Only a few papers have reported supersaturated solutions with long-term stability over the scale of several days.

EUDRAGIT®, which is a methacrylic acid copolymer, has various characteristics depending on its substituents. EUDRAGIT® has been widely used as a pharmaceutical excipient for enteric film-coating formation, sustained release, taste/smell masking, and wear/moisture prevention. Solid dispersions using these polymers as carriers have been documented (19–21).

Nuclear magnetic resonance (NMR) spectroscopy is an important technique that allows direct observation at the molecular level of both low-molecular-weight compounds and macromolecules. In the last 25 years, solid-state NMR has increasingly evolved thanks to the development of magic-angle spinning (MAS), cross polarization (CP), and high-power decoupling (21). In the pharmaceutical field, the solid-state NMR technique is used for studying structure/conformation, analyzing molecular motions, assigning resonances, and measuring internuclear distances (22). Solid-state ^{13}C-NMR studies have revealed that the solid-state interactions of probucol/polyvinylpyrrolidone (PVP) and PVP/sodium dodecyl sulfate (SDS) on grinding play a key role in probucol nanoparticle formation (23). Multivariate analysis of solid-state ^{13}C-NMR spectra of troglitazone/PVP dispersions have allowed prediction of the drug's recrystallization behavior (24). In particular, NMR relaxation time can provide information on the molecular motions of specific atoms in a molecule. Therefore, it is a powerful tool for determining individual molecular motions in multicomponent systems such as pharmaceutical formulations (25). Schantz *et al.* evaluated the physical stability of amorphous binary mixtures of citric acid and paracetamol by relaxation time measurement (26), and Aso *et al.* reported that the miscibility of a drug and an excipient in solid dispersion can be evaluated by assessing its relaxation decay (27). Solid dispersions of ibuprofen or flurbiprofen with EUDRAGIT® RL100 have also been evaluated by ^{1}H relaxation time measurement (20). These reports confirm the utility of solid-state NMR for the analysis of pharmaceutical formulations that include solid dispersion. In contrast, there have been few reports describing the molecular state of solid dispersions in aqueous media by solution-state NMR measurement because supersaturated solutions from solid dispersion are usually viscous, weak in concentration, and unstable for the time scale needed for NMR measurement. If these difficulties could be overcome by applying NMR techniques to long-stabilized supersaturated solutions, detailed structural information could be obtained. The combination of solution- and solid-state NMR spectroscopy could provide us with a deep understanding of solid dispersion because the molecular states both before and after dispersing in aqueous media could be evaluated.

In this study, a highly stable solid dispersion and highly concentrated supersaturated solution were prepared by utilizing cryogenic grinding of mefenamic acid (MFA) and EUDRAGIT® EPO (EPO) as a model of a poorly water-soluble drug and carrier polymer, respectively. An *in vitro* dissolution test and an *in vivo* oral absorption study in rats were performed to investigate the dissolution characteristics and the gastrointestinal absorption rate of MFA in supersaturated solution. The physicochemical properties of the solid dispersion were assessed by powder x-ray diffraction (PXRD), infrared (IR), and solid-state NMR including relaxation time measurement, to investigate the formation and stabilization mechanisms. Furthermore, solution-state NMR measurement was performed to investigate the molecular state of MFA and EPO in the supersaturated solution.

MATERIALS AND METHODS

Materials

MFA (MW: 241.29), indomethacin (IMC; MW: 357.79), and piroxicam (PXC; MW: 331.25) were purchased from Wako Pure Chemical Industries, Ltd. (Osaka, Japan). Aminoalkyl methacrylate copolymer E, EUDRAGIT® EPO (EPO; mean MW: 135,000) and methacrylic acid copolymer L, EUDRAGIT® L100 (L100; mean MW: 150,000) were kindly provided by Evonik Degussa Japan Co. Ltd. (Tokyo, Japan). All materials were of chemical grade and were used as received. All other regents were commercially available and of analytical grade. The molecular structures of MFA, EPO, and L100 are shown in Fig. 1.

Preparation of Solid Dispersions

Solid dispersions were prepared by the cryogenic grinding method. Drug and polymer were mixed at a weight ratio of 24/76 to obtain a physical mixture (PM). The PM was ground in a TI-500ET vibration rod mill (CMT Co. Ltd., Fukushima, Japan) at −180°C for 90 min to prepare cryogenic-ground mixture (Cryo-GM).

Powder X-Ray Diffractometry

PXRD measurements were performed using a Miniflex II X-ray diffractometer (Rigaku, Tokyo, Japan) with the temperature at 25°C, voltage at 30 kV, current at 15 mA, scanning speed at 4°/min, and CuKα radiation source with a Ni filter.

In Vitro Dissolution Test

Dissolution tests were carried out at 37.0±0.5°C for 180 min in 500 mL of 0.1 M acetate buffer (pH 5.5) using a USP type 2 apparatus NTR-VS6P (Toyama Sangyo, Osaka, Japan) with the paddle speed at 100 rpm. Samples containing 250 mg of drug were put into the dissolution vessel. Five milliliters of dissolution medium were withdrawn at the indicated periods (1, 3, 5, 7, 10, 15, 20, 25, 30, 60, 120, and 180 min) and immediately filtered by a 0.20 μm ADVANTEC® membrane filter (Tokyo Roshi Kaisha, Tokyo, Japan). The filtrate was diluted and analyzed with a V-650 UV–vis Spectrometer (JASCO, Tokyo, Japan). The determinations of MFA, IMC, and PXC concentrations were performed at λ=345, 340, and 251 nm, respectively. In the meantime, an equal volume of the same medium was added to maintain constant volume. The dissolution data were obtained in triplicate.

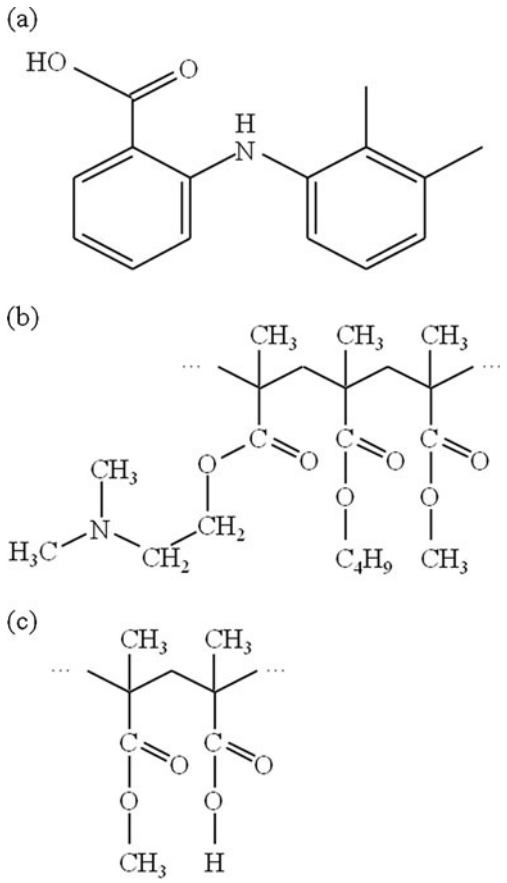

Fig. 1 Molecular structures of (**a**) MFA, (**b**) EUDRAGIT® EPO, and (**c**) EUDRAGIT® L100.

Animals

All experiments were conducted according to guidelines approved by the Nihon University Animal Care and Use Committee (Nihon University, Japan). Adult male Wistar/ST rats (8 weeks old, 230–250 g body weight) were obtained from Japan SLC, Inc. (Shizuoka, Japan). The rats were housed in stainless steel cages with a 12 h light/dark cycle (light on from 8:00 am to 8:00 pm) under conditions of controlled temperature maintained at 25°C ± 1°C with a humidity of 55% ± 10% relative humidity (RH) for at least 1 week before use. Animals were fasted for 15 h prior to the experiments.

In Vivo Absorption Studies

Intact MFA was suspended in 0.5% carboxymethylcellulose (CMC) solution to prepare a 10 mg/mL dosing solution. PM or Cryo-GM (10 mg as MFA) was dispersed in 1 mL of 0.1 M acetate buffer solution (pH 5.5). The dosing solution at a dose of 2 mL/kg body weight was administered orally by gavage to rats. The dose was calculated to be 20 mg/kg as MFA. At the designated time points (0.5, 1, 2, 4, 6, 10, and 24 h after the administration of the drug, blood (0.5 mL) was collected from the jugular vein under pentobarbital anesthesia (40 mg/kg). The blood was centrifuged to separate the plasma. Each plasma sample was stored at −20°C until analysis.

Determination of MFA Concentrations in Plasma

Plasma concentrations of MFA were determined by a minor modification of the high-performance liquid chromatography (HPLC) method reported previously (28,29). Briefly, 50 μL of plasma sample in a 1.5 mL test tube was added 20 μL of methanol solution containing diclofenac (5 μg/mL) to serve as an internal standard. After acidification with 10 μL of 0.1 N HCl, the mixture was extracted with 1 mL of hexane/diethyl ether (50/50, v/v) by mechanical shaking for 5 min. After centrifugation at 11,400×*g* (12,000 rpm) for 10 min at 4°C, the upper organic solvent layer was transferred to another tube. The residue mixture was extracted again with 1 mL of hexane/diethyl ether. The organic solvent was evaporated to dryness at 30°C. The evaporated residue was reconstituted

with 200 μL of the HPLC mobile phase, and an aliquot of 20 μL was analyzed by using the HPLC apparatus (Shimadzu, Kyoto, Japan). The analytical column, C-18 CAPCELL PAK® (4.6×250 mm, 5 μm, Shiseido, Tokyo, Japan) was used at 40°C. The mobile phase of acetonitrile/0.05 M phosphate buffer (pH 7.5) (30/70, v/v) was pumped at a flow rate of 1.0 mL/min, and the column eluate was monitored at 280 nm. The retention times were 10.7 min for the internal standard and 12.8 min for MFA. The limit of detection was 10 ng/mL of MFA in plasma. Peakarea ratios for MFA relative to the internal standard were linearly related (r^2=0.998) to the amount of MFA added to blank plasma in the range of 100–8,000 ng/mL. The intra- and inter-day assay coefficients of variation were calculated to be less than approximately 3% in concentrations ranging from 150 to 8,000 ng/mL. The mean analytical recovery was 95.3% in that range.

Pharmacokinetic Analysis

The highest plasma concentration of MFA was employed as C_{max}, and the time to reach C_{max} was defined as t_{max}. The area under the plasma concentration *versus* time curve (AUC) was calculated from 0 to 24 h using a linear trapezoidal rule.

Fourier Transform IR (FT-IR) Spectroscopy

IR spectroscopy measurement was performed with a FT-IR 300E spectrometer (JASCO, Tokyo Japan) using the KBr disk method. The IR spectra were obtained in the scan range of 650–4,000 cm^{-1} at a resolution of 4 cm^{-1} with 32 scans at a temperature of 25°C.

Solid-State NMR Spectroscopy

All solid-state NMR measurements were conducted using a JNM-ECA600 NMR spectrometer (JEOL, Tokyo, Japan) with a magnetic field of 14.09 T operating at the ^{1}H Larmor frequency of 600.0 MHz and the ^{13}C frequency of 150.0 MHz. Samples (ca. 100 mg) were placed as powders into 4 mm silicon nitride rotors. The ^{13}C spectra were acquired using CP together with MAS at 15.0 kHz and high-power ^{1}H decoupling at an inlet air temperature of 25.0°C. For each spectrum, the total number of accumulations (1,000–4,096) was acquired depending on the required signal-to-noise ratio. Pertinent acquisition parameters included relaxation delays of 2–16 s, a CP contact time of 5 ms, and a ^{1}H 90° pulse of 2.7 μs. The total number of data points was 4,096 points per spectrum in each experiment, zero-filled to 16,384 points. All spectra were externally referenced to tetramethylsilane by setting the methine peak of hexamethylbenzene to 17.3 ppm. Spinning sidebands were confirmed by changing the rotational speed from 10.0 to 15.0 kHz. ^{1}H spin–lattice relaxation time (T_1) was measured using the standard $[180°\text{-}\tau\text{-}90°]_n$ inversion recovery method with ^{1}H 90° pulse of accurately determined for each sample; ^{13}C-T_1 was determined using a pulse sequence reported by Torchia (30).

Solution-State NMR Spectroscopy

All solution NMR measurements were performed using the JNM-ECA600 NMR spectrometer described in the previous section. Solution-state NMR samples, except unprocessed MFA, were dissolved at a concentration of 3 mg/mL as MFA in 0.1 M acetate buffer (pH 5.5), which was prepared by using D_2O and put in glass sample tubes (5 mmϕ). Due to the low solubility of MFA at pH 5.5, unprocessed MFA was dissolved in $CDCl_3$. ^{1}H NMR spectra were recorded at 37.0°C using a relaxation delay of 5 s, ^{1}H 45° pulse of 7.75 μs, spectral width of 15 ppm centered at 5.0 ppm, and spinning rate of 15 Hz. The signal of the solvent was used for ^{1}H chemical shift referencing ($CHCl_3$ for 7.25 and HDO for 4.67 ppm). For each spectrum, the total number of accumulations (32–128) was acquired depending on the required signal-to-noise ratio. ^{1}H-T_1 was measured using the standard $[180°\text{-}\tau\text{-}90°]_n$ inversion recovery method. ^{1}H difference nuclear Overhauser effect (NOE) experiments were applied to the same Cryo-GM solution sample. A difference NOE spectrum was obtained by subtracting a pair of spectra ($\Delta I = I_{on}\text{-}I_{off}$) acquired in an interleaved fashion. On- and off-resonance frequencies were at 8.00 ppm and −10.0 ppm, respectively; the measurements were conducted without sample spinning. Pertinent acquisition parameters included a relaxation delay of 5 s, ^{1}H 90° pulse of 13.5 μs, total accumulation number of 512, NOE build-up time of 3 s, and irradiation attenuators varying from 65 to 77 dB.

RESULTS AND DISCUSSION

Effect of EUDRAGIT® Species on Formation of MFA Solid Dispersion

Two types of EUDRAGIT®, EPO and L100, were used as polymer carriers to investigate the effect of substituents on the formation of solid dispersions with MFA. Because of the low glass transition temperature of EPO, we utilized cryogenic conditions. Solid dispersions of MFA and EUDRAGIT® at the weight ratio of 24/76 were therefore prepared by the cryogenic grinding method. Figure 2 shows the PXRD patterns of MFA/EPO and MFA/L100 systems. Unprocessed MFA (Fig. 2a) showed sharp X-ray diffraction peaks, which were attributed to its crystalline state. L100 (Fig. 2b) and EPO (Fig. 2e) showed no peaks due to their amorphous structures. The PXRD pattern of each PM (Fig. 2c and f) showed a superposition of the crystalline MFA and polymer patterns.

The peaks of crystalline MFA had completely disappeared in the Cryo-GM with EPO (Fig. 2g). This result indicates that crystalline MFA was transformed into the amorphous state by cryogenic grinding with EPO. In contrast, diffraction peaks derived from crystalline MFA were observed in the Cryo-GM with L100 (Fig. 2d). EPO can works as proton acceptor because it contains a tertiary amino group in addition to a carbonyl group in the structure. Hence, EPO can form strong interactions with MFA as proton donor. On the other hand, in the present study, almost no intermolecular interaction was formed between MFA and L100, which lacks the amino group. These results suggest that the aminoalkyl group in the side chain of EPO plays an important role in the amorphization of MFA. Figure 2h shows the diffraction pattern of the MFA/EPO Cryo-GM after 10 months' storage at 25°C 75% RH. MFA/EPO Cryo-GM maintained its amorphous state for 10 months under this condition, indicating high stability of its solid dispersion. We therefore concluded that a highly stable amorphous solid dispersion of MFA could be obtained by cryogenic grinding with EPO.

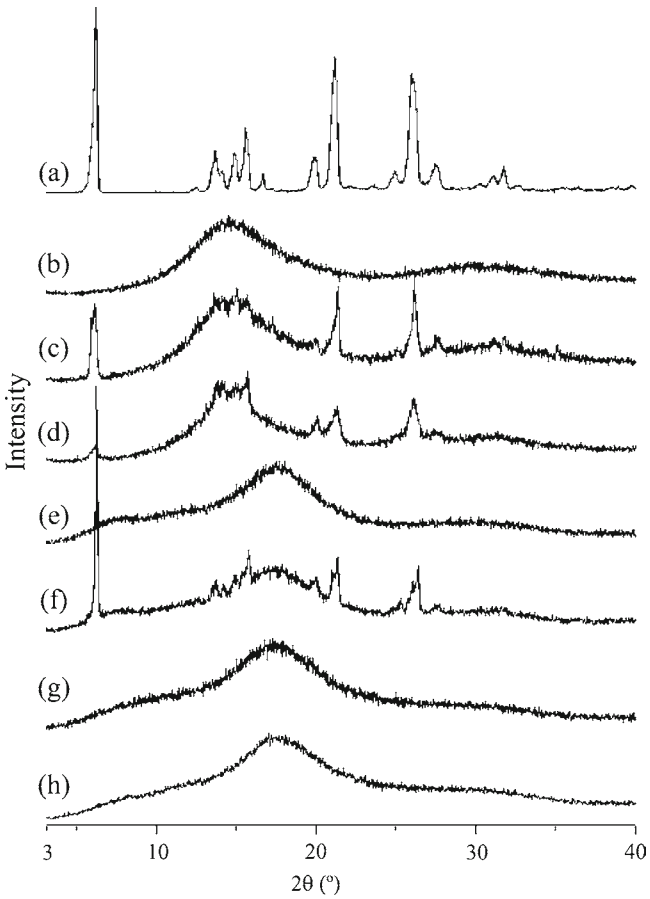

Fig. 2 PXRD patterns of (**a**) MFA, (**b**) L100, (**c**) MFA/L100 PM, (**d**) MFA/L100 Cryo-GM, (**e**) EPO, (**f**) MFA/EPO PM, (**g**) MFA/EPO Cryo-GM, and (**h**) MFA/EPO Cryo-GM stored at 25°C, 75% RH, for 10 months. The weight ratios of the binary mixtures are 24/76.

In Vitro Dissolution of MFA from MFA/EPO Cryo-GM

Dissolution tests were performed to investigate the dissolution property of MFA from MFA/EPO Cryo-GM in 0.1 M acetate buffer (pH 5.5). Figure 3 shows the dissolution profiles of MFA in the MFA/EPO system. Unprocessed MFA reached to its solubility (2.2 μg/mL) in 30 min. PM gradually released MFA and showed an MFA concentration of 160 μg/mL after 3 h. In the MFA/EPO Cryo-GM, MFA dissolved rapidly into the medium, and clear supersaturated solution was formed within an hour. The drug concentration of the supersaturated solution (488 μg/mL) was more than 200 times greater than that of crystalline MFA. The supersaturated solution was maintained over 1 month at room temperature (data not shown). Such a highly stable supersaturated solution has not been previously reported. Generally, a supersaturated drug solution is thermodynamically unstable and has a tendency to return to the equilibrium state in accordance with drug precipitation. Precipitation inhibitors such as polymers and surfactants are necessary to prevent recrystallization of drugs and to maintain the supersaturated state. Raghavan *et al.* (31) reported that the stabilization mechanism of a supersaturated solution of hydrocortisone acetate and hydroxypropyl methylcellulose was the increased activation energy for nucleation due to hydrogen bonds between drug molecules and the polymer. Based on these results, we concluded that the stability of the supersaturated solution from the MFA/EPO Cryo-GM was attributed to the specific intermolecular interaction between MFA and EPO, which was formed by the cryogenic grinding process. PM also showed rather improved dissolution of MFA. It was suggested that in the PM, the formation of the intermolecular interactions between MFA and EPO occurred during the process of dissolution, resulting in the slow and partial dissolution of MFA, in contrast to the rapid and complete dissolution of MFA/EPO Cryo-GM.

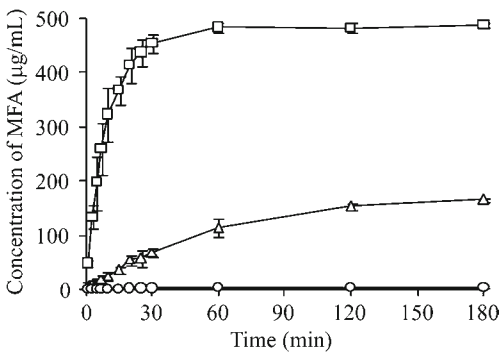

Fig. 3 Dissolution profiles of (○) MFA, (Δ) MFA/EPO PM, and (□) MFA/EPO Cryo-GM in 0.1 M acetate buffer at pH 5.5 (n=3, mean ± SD).

In Vivo Oral Absorption

In vivo oral absorption of MFA from the Cryo-GM solution was evaluated in rats. The plasma concentration–time profiles following a single oral administration of MFA (in 0.5% CMC aqueous solution), MFA/EPO PM (in acetate buffer), and MFA/EPO Cryo-GM (in acetate buffer) are shown in Fig. 4. The drug plasma concentrations of MFA and PM suspensions did not show an obvious maximum drug concentration because of the low concentration of MFA in plasma. On the other hand, administration of MFA/EPO Cryo-GM solution resulted in a significantly increased plasma concentration of MFA at 2 h after administration. AUCs until 24 h were 1,510 ± 510 ng·h/mL in MFA suspension, 3,465 ± 592 ng·h/mL in MFA/EPO PM suspension, and 11,794 ± 399 ng·h/mL in Cryo-GM solution. MFA/EPO Cryo-GM solution exhibited 7.8- and 3.4-fold higher AUCs compared to MFA and MFA/EPO PM suspensions, respectively; moreover, MFA/EPO Cryo-GM solution showed clearly improved absorption characteristics compared with those of MFA and MFA/EPO PM suspensions. These results could be due to the increased solubility of the poorly water-soluble drug shown in Fig. 3. Since MFA is classified as a BCS class II drug having high permeability and low solubility, its absorption is governed by the dissolution process of the drug in the gastrointestinal tract. In MFA/EPO Cryo-GM solution, the dissolution process did not limit the rate of MFA absorption because all MFA molecules were immediately dissolved. In addition, the MFA/EPO Cryo-GM solution was stable during the process of dissolution. Thus, absorption of MFA from the MFA/EPO Cryo-GM solution may depend on the membrane permeation process. The MFA/EPO Cryo-GM solution improved the peroral bioavailability of MFA due to its high permeability. From these results, it was revealed that solid dispersion with EPO was intrinsically effective for the improvement of oral absorption of MFA.

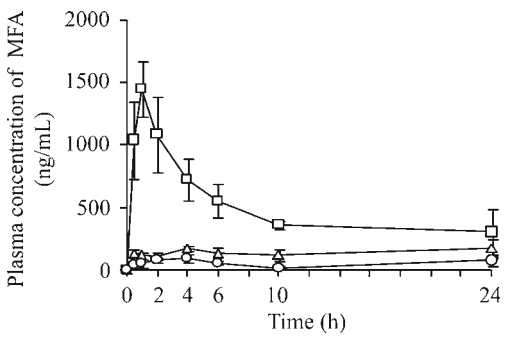

Fig. 4 Plasma concentration–time profiles of MFA in adult male Wistar/ST rats (8 weeks old, 230–250 g body weight) after a single oral administration of (○) MFA suspension, (△) PM suspension, and (□) Cryo-GM solution at a dose of 20 mg/kg as MFA. Mean AUCs until 24 h were 1,510 ± 510 ng·h/mL from MFA suspension, 3,465 ± 592 ng·h/mL from MFA/EPO PM suspension, and 11,794 ± 399 ng·h/mL from MFA/EPO Cryo-GM solution (n=3–4, mean ± SE).

IR Spectroscopy

To evaluate molecular interactions between MFA and EPO in the solid state, IR spectroscopy was used (Fig. 5). The spectra of the pure materials showed characteristic absorption peaks due to the different functional groups. In the spectra of MFA, stretching modes of N-H, C=O, and C=C were specific for MFA and were recorded at approximately 3,308 cm^{-1}, 1,650 cm^{-1}, and 1,576 cm^{-1}, respectively (Fig. 5a and e) (32). In these wave number regions, EPO showed only 1 peak originating from the C=O stretching vibration at 1,730 cm^{-1} (Fig. 5b and f). In MFA/EPO PM, these peaks were observed at the same wave numbers as those shown by their individual components (Fig. 5c and g). After cryogenic grinding, the peak derived from the N-H stretching vibration shifted to the lower wave number (3,261 cm^{-1}), and line broadening was observed (Fig. 5d). The C=O stretching vibration of MFA might be overlapped with the C=O stretching vibration in EPO according to the high wave number shift. The C=C stretching vibration was also shifted to a higher wave number (1,582 cm^{-1}) (Fig. 5h).

Further investigation was performed in order to mention that the changes in IR spectrum of MFA in MFA/EPO Cryo-GM were not the result of merely amorphization but formation of some intermolecular interaction with EPO. We tried to prepare amorphous MFA without EPO. Melt-quenching method was not appropriate for preparing amorphous MFA because MFA started to decompose immediately after the fusion around 230°C (33). Cryogenic grinding method and solvent evaporation method using methanol and dichloromethane were used. However, PXRD measurement showed that amorphous MFA was not formed according to those methods (data not shown). Hence, it was suggested that amorphous MFA could not form without adding additives at room temperature.

Since it was difficult to prepare amorphous MFA without additive, we prepared another solid dispersion of MFA with hydroxypropyl methylcellulose (HPMC, Fig. S1) by cryogenic grinding method and compared its IR spectrum with that of MFA/EPO Cryo-GM. PXRD pattern of MFA/HPMC Cryo-GM at a weight ratio of 24/76 showed hallo pattern (Fig. S2). IR measurement showed that the peak positions in MFA/HPMC PM were the superimposition of those in unprocessed MFA and HPMC (Fig. S3). In the IR spectrum of MFA/HPMC Cryo-GM, N-H stretching vibration peak of MFA did not change, while the C=O stretching vibration peak of MFA showed peak broadening and small shift to a higher wave number at 1,657 cm^{-1}. The spectral changes were due to the overlap of two peaks: an unshifted one at 1,650 cm^{-1} and another shifted one around 1,680 cm^{-1}. This result suggested the limited drug-polymer miscibility; non-interacted small crystalline MFA, which was not observed by PXRD measurement, coexisted with interacted MFA with HPMC (34). It was emphasized that the peak shift of C=O stretching vibration from

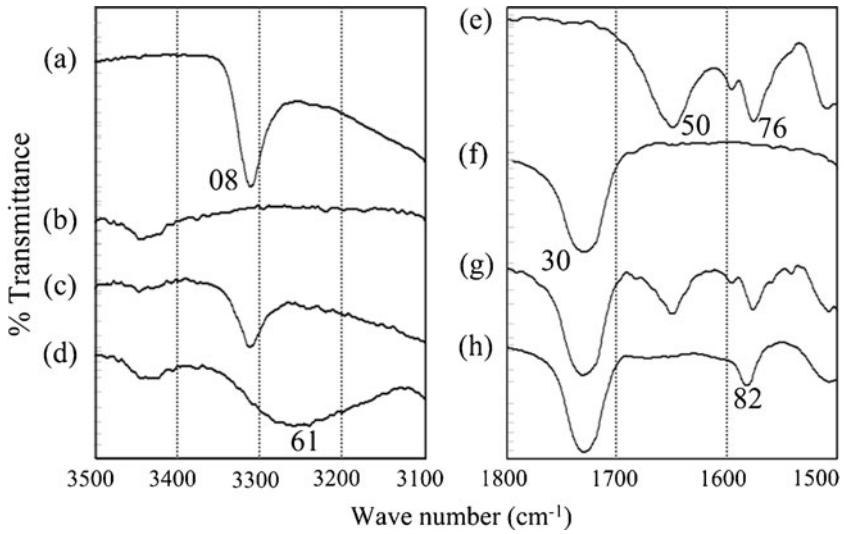

Fig. 5 IR spectra of (**a**, **e**) MFA, (**b**, **f**) EPO, (**c**, **g**) MFA/EPO PM, and (**d**, **h**) MFA/EPO Cryo-GM. (**a**–**d**) and (**e**–**h**) show the spectra at 3,500–3,100 cm^{-1} and 1,800–1,500 cm^{-1}, respectively.

PM to Cryo-GM was much larger in MFA/EPO system than in MFA/HPMC system, even when only the peak of interacted MFA with HPMC around 1,680 cm^{-1} was taken into consideration. The peak shift on the formation of molecularly-mixed solid dispersion should be derived from the breakage of drug crystal packing and subsequent arising new intermolecular interaction of drug with polymer (34). The remarkable difference in the peak position between MFA/EPO Cryo-GM and MFA/HPMC Cryo-GM could be derived from the strength of intermolecular interaction between drug and polymer. It was concluded that carboxyl group of MFA could strongly contribute to the intermolecular interactions with EPO in the Cryo-GM.

As shown in Fig. 2, aminoalkyl groups in EPO played an important role in the formation of intermolecular interactions with MFA. Since an aminoalkyl group is a proton-accepting functional group, it is reasonable that the proton-donating carboxyl group of MFA (where large peak shift was observed in IR spectroscopy) worked as the counterpart of the aminoalkyl groups of EPO. It was suggested that strong intermolecular interactions could occur between MFA and EPO in the Cryo-GM, such as electrostatic interaction or hydrogen bonding in addition to hydrophobic interaction.

Solid-State ^{1}H-T_1 Measurement

The solid-state NMR technique was utilized for further investigation of the molecular states of the MFA/EPO solid dispersion. Solid-state ^{1}H-NMR measurement was performed for MFA, EPO, PM, and Cryo-GM. Since little change in peak shape and chemical shift was observed between PM and Cryo-GM (data not shown), we cannot evaluate or discuss the molecular state of each sample appropriately. Changes in peak shape and shift should be due to line broadening and overlaps of the ^{1}H signals. Table I shows the ^{1}H-T_1 values of the samples as measured by the inversion recovery method. NMR relaxation time provides information on molecular mobility while the chemical shift in the NMR spectrum shows the chemical environment of the molecules. The ^{1}H-T_1 of MFA was 15.4 s, reflecting its low molecular mobility resulting from its high crystallinity. EPO exhibited a very short ^{1}H-T_1 of 1.0 s, indicating high molecular mobility emerging from its flexible polymeric structure. The magnetization recovery of MFA/EPO PM can be described with a bi-exponential equation, giving 2 ^{1}H-T_1 values of 16.7 and 0.9 s. On the other hand, the magnetization recovery pattern for MFA/EPO Cryo-GM is mono-exponential, with a single ^{1}H-T_1 value of 1.0 s. In solid samples, since T_1 is much longer than spin-spin relaxation time (T_2), excited energy in the spin system will be retained for a fairly long time before transferring magnetization to the magnetic lattice (35,36). During this holding process, spin energy propagates among the neighboring nuclei through "flip-flop" of the magnetization without any loss of energy. This process, known as spin diffusion, tends to average the relaxation times of the different protons in a sample to a single value. The averaging effect is complete in the case of a sample homogeneous solid while different relaxation times can be measured for protons belonging to different domains. The averaging effect permits estimation of the heterodomain's average size, considering Eq. 1 for diffusion in 3 dimensions (37).

$$L = \sqrt{6D_s t_1} \tag{1}$$

where L is the average diffusion path length occurring in a time t_1, and D_s is the diffusion coefficient. The L value was calculated

Table I ^{1}H-T_1 of MFA/EPO System in Solid State

Sample	^{1}H-T_1 (s)
MFA	15.4
EPO	1.0
PM	16.7, 0.9
Cryo-GM	1.0

to be around 200–300 Å by applying T_1 experimental values and a typical D_s (6×10^{-16} m^2/s) for solid polymers (21,37). Taking the effects of spin diffusion into account, a single ^1H-T_1 value in MFA/EPO Cryo-GM implies that MFA and EPO existed within a distance of at least 200–300 Å. On the other hand, the 2 different ^1H-T_1 values shown in the PM indicated that the domains of MFA and EPO were separated by more than 300 Å from each other. It is possible that amorphous MFA having no interaction with EPO showed the ^1H-T_1 at 1 s incidentally. However, PXRD measurements confirmed that cryogenic-grinding of only MFA without EPO did not give the amorphous MFA (data not shown). This result indicated that amorphous MFA without interaction to EPO should not exist in the MFA/EPO Cryo-GM, and the observed changes of ^1H-T_1 of MFA derived from the cryogenic grinding process of MFA with EPO. From the result of our ^1H-T_1 measurements, it was revealed that MFA and EPO mixed homogeneously through intermolecular interactions in the Cryo-GM.

Solid-State ^{13}C-CP/MAS NMR Spectroscopy

To investigate the molecular state of MFA/EPO solid dispersion in detail, solid-state ^{13}C-CP/MAS NMR measurement was conducted. Solid-state ^1H-NMR evaluation is difficult in multicomponent samples since the narrow resonant frequency band of ^1H has a tendency to superimpose the ^1H signals. On the other hand, ^{13}C has a wider resonant frequency band compared with ^1H, so it is possible to evaluate the individual nuclei in the molecule whether it is multicomponent or not (Fig. 6). The numbers in the spectrum correspond to the carbons in the molecular structure (38). In the present study, MFA showed characteristic peaks in 3 regions, 10–30 ppm, 100–160 ppm, and 170–180 ppm where peaks derived from methyl groups, aromatic rings, and a carbonyl group were observed (Fig. 6a). For EPO, the peaks were assigned using a two-dimensional NMR technique in solution state (data not shown). Carbonyl carbon in the side chain was recorded at 177.7 ppm, and the other carbons in the main and side chains were detected between 10 and 80 ppm (Fig. 6b). More precisely, peaks derived from alkyl chains were sorted into 3 kinds of carbons: those neighboring oxygen, nitrogen, and other carbon atoms. According to the theory of electron density, these carbons should be observed in low-to-high magnetic field regions in the order of decreasing electronegativity of the neighboring atom. This prediction is in good agreement with the results of our two-dimensional NMR measurements.

To clarify the molecular state of MFA, we focused on the region from 100 to 160 ppm. In the spectrum of MFA/EPO Cryo-GM, significant peak broadening was observed, compared with that of MFA/EPO PM (Fig. 6c and d). Peak broadening in the solid-state NMR spectrum could be ascribable either to a wider distribution of isotropic chemical shifts for the same carbons belonging to different molecules, or to an equable suppression of the molecular mobility of the carbons (20). Mobility of MFA molecules was significantly enhanced in the Cryo-GM, as discussed in the results of ^1H-T_1 measurement. Therefore, this line broadening was explained in terms of a wider distribution of chemical environments of the same carbons in different molecules due to the amorphous nature of the solid dispersions where drugs existed in various conformational situations (20).

The changes in chemical shift were discussed in order to observe the interaction of MFA and EPO. In the spectrum of MFA/EPO PM, all peaks were observed at the same position as in each individual constituent (Fig. 6c). On the other hand, the changes of chemical shift with peak broadening were observed in the spectrum of MFA/EPO Cryo-GM (Fig. 6d). The degree of peak shift in the aromatic ring that contained the carboxyl group (C1-C6) appeared to be greater than those of the other aromatic carbons (C1′-C6′). This implies that the electron density of the aromatic ring with a carboxyl group could be dramatically changed because of the strong intermolecular interaction via carboxyl groups. As for the spectrum of EPO, the peak derived from N-methyl and N-methylene carbons neighboring to nitrogen atoms shifted. These results in the CP/MAS spectra were consistent with the changes observed in the IR spectra, indicating the formation of intermolecular interaction between the carbonyl group of MFA and the aminoalkyl group of EPO. We therefore concluded that MFA molecules were monomolecularly dispersed in the EPO polymer matrix via intermolecular interactions.

Solid-State ^{13}C-T_1 Measurement

Protons are almost 100% in natural abundance, and spin diffusion with nearby protons is the major relaxation pathway. ^1H-T_1 reflects averaged and whole molecular mobility in a sample. In contrast, ^{13}C is resistant to the homonuclear spin diffusion effect because the natural abundance of ^{13}C, i.e., 1%, is so small (39). Since dipole-dipole interaction with the protons directly bound to ^{13}C is the dominant relaxation pathway of excited ^{13}C, ^{13}C-T_1 values provide information about localized molecular mobility (40). Here, we measured ^{13}C-T_1 to evaluate changes in the localized molecular motions of each individual component on the formation of the solid dispersion. Table II shows ^{13}C-T_1 values for MFA, EPO, and MFA/EPO Cryo-GM as determined by the Torchia method. MFA showed an extremely long ^{13}C-T_1 of over 400 s and the ^{13}C-T_1 should be in the slow motional regime of T_1 minimum; this shows its rigid crystalline property, except for the methyl groups with high molecular mobility. On the contrary, EPO showed smaller ^{13}C-T_1 values reflecting rather high molecular mobility. The ^{13}C-T_1 values of the alkyl chains, the terminal groups (aminoalkyl groups and O-methyl group) and the

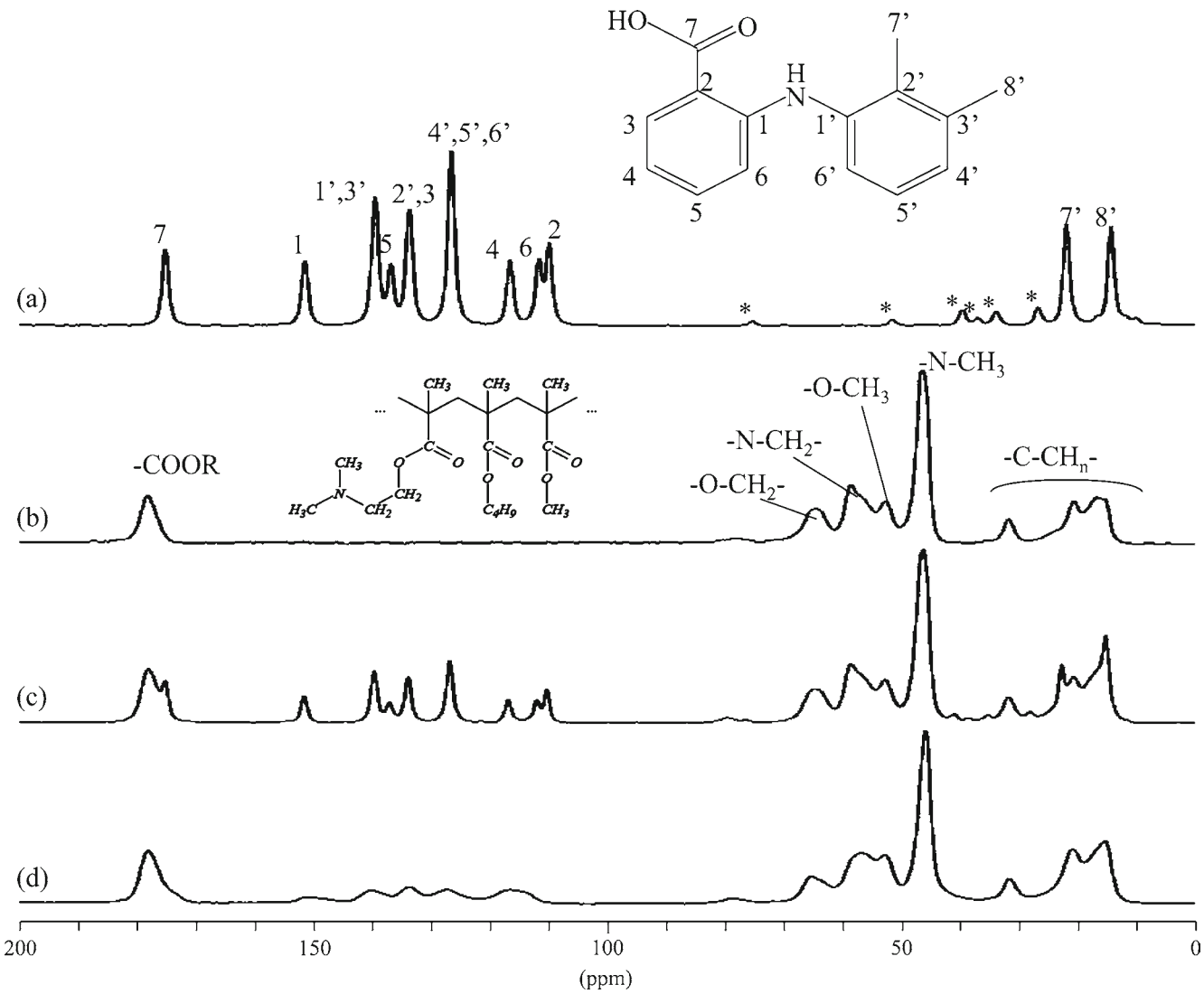

Fig. 6 ^{13}C-CP/MAS NMR spectra of (**a**) MFA, (**b**) EPO, (**c**) MFA/EPO PM, and (**d**) MFA/EPO Cryo-GM. Asterisk (*) shows the spinning side bands.

carbonyl carbon were 0.5–1.3 s, 2.4–11.7 s and 18.6 s, respectively. Ethylene-dimethylaminoethyl methacrylate copolymer, a composition of EPO, was known as semicrystalline polymer (41). Solid state NMR study in the reported article indicated that dimethylamino groups of this copolymer were in non-crystalline state and mostly located outside the crystalline regions of alkyl chains (41). Thus, at least ^{13}C-T_1 of terminal groups in EPO could be in the extremely narrowing region of T_1 minimum, since carbons at the terminal groups showing higher ^{13}C-T_1 value were more mobile than alkyl chains in polymer backbone. It was confirmed that the half width of the peaks reflecting the molecular mobility was sharper in the terminal groups than that of alkyl chains.

In MFA/EPO Cryo-GM, ^{13}C-T_1 values of MFA within the slow motional region were significantly shortened compared with the unprocessed sample, indicating its amorphous nature with high molecular mobility. Meanwhile, EPO in the Cryo-GM within the extremely narrowing region showed longer ^{13}C-T_1 values than did the raw material. It has been reported that in the case of nifedipine-PVP and phenobarbital-PVP solid dispersions, the mobility of PVP carbonyl carbon was changed by hydrogen bond interactions, resulting in the change of ^{13}C-T_1 of PVP carbonyl carbon (42). Especially, ^{13}C-T_1 values at 58.0 and 45.9 ppm, which were assigned to the ^{13}C next to nitrogen, were greatly changed. The formation of intermolecular interaction with MFA via the aminoalkyl group increased the localized motion of carbon atoms. These results correspond well with the chemical shift changes of ^{13}C-CPMAS NMR spectra. We concluded that in MFA/EPO Cryo-GM, MFA had extremely high molecular mobility compared to its crystalline state, and EPO formed intermolecular interaction via the aminoalkyl group, resulting in the changes of localized molecular mobility.

Table II ^{13}C-T_1 of MFA/EPO System in Solid State

^{13}C Assignment (ppm)		T_1 (s)	
		Intact	Cryo-GM
MFA	C7 (174.6)	— [a]	— [b]
	C1 (151.0)	— [a]	— [a]
	C1′, C3′ (139.1)	465.9	35.6
	C5 (136.4)	898.2	31.9
	C2′, C3 (133.3)	699.0	27.8
	C4′, C5′, C6′ (126.2)	578.0	15.5
	C4 (166.2)	481.9	24.3
	C6 (111.3)	682.7	24.3
	C2 (109.7)	913.1	24.3
	C7′ (22.0)	3.2	— [b]
	C8′ (14.4)	47.6	— [b]
EPO	COOR (177.7)	18.6	22.2
	-O-CH_2- (64.0)	0.9	1.0
	-N-CH_2- (58.0)	2.4	13.6
	-O-CH_3 (52.1)	11.7	11.9
	-N-CH_3 (45.9)	4.0	10.2
	-C-CH_n- (31.2)	0.5	0.5
	-C-CH_n- (22.0)	0.5	0.9
	-C-CH_n- (14.4)	1.3	3.4

[a] Accurate value was not acquired because of overlong relaxation time.

[b] Value was not obtained because of overlaps of the signals.

Solution ^{1}H-NMR Measurement

^{1}H-NMR measurement was performed to evaluate the molecular state of MFA in supersaturated solution. Figure 7 shows ^{1}H-NMR spectra of (a) MFA in $CDCl_3$, (b) EPO in acetate buffer, and (c) MFA/EPO Cryo-GM in acetate buffer. MFA dissolved in $CDCl_3$ shows some characteristic peaks (38). Signals at 2.18 and 2.33 ppm were assigned to the 2 kinds of methyl protons. In the low magnetic field region, peaks originating from protons of aromatic rings were observed between 6.66 and 8.01 ppm. The weak and broad peak at 9.10 ppm was assigned to the exchangeable proton of the secondary amino group. Except for the signal of the secondary amino group, all the signals arising from dissolved MFA were very sharp, indicating that MFA molecules demonstrated high molecular mobility when they were monomolecularly dispersed in $CDCl_3$ solution. On the other hand, the peaks shown on the spectrum of EPO in acetate buffer showed broad line widths. This is because EPO with a molecular weight of 150,000 exhibits low molecular motion even when it is dissolved in acetate buffer solution. The peak assignments were clarified by two-dimensional NMR measurement in $CDCl_3$ (data not shown). In the spectrum of MFA/EPO Cryo-GM, distinct peaks derived from the MFA molecule were clearly observed at low magnetic field range, although the peak shapes were comparatively broader than those in $CDCl_3$ solution. In contrast, no peak was observed when MFA itself was dispersed in acetate buffer because of the low solubility of MFA (data not shown). Solution NMR can detect only signals arising from nuclei with high mobility, and no signal can be observed when the mobility of subject nuclei is suppressed, as in the crystalline state (43). These results supported the concept of MFA solubility enhancement due to the formation of solid dispersion with EPO, as shown in Fig. 3. We speculated that in MFA/EPO Cryo-GM solution, MFA existed not as a nanocrystalline state but as a monomolecularly dispersed one, although the molecular mobility of MFA was suppressed compared with that in $CDCl_3$ solution. We tried to determine the particle size of MFA in MFA/EPO Cryo-GM solution by dynamic light scattering measurement using Microtrac UPA® (Nikkiso Co., Ltd., Tokyo, Japan; the detection rage of 0.8 nm–6.5 μm). However, light scattering intensity of MFA/EPO Cryo-GM solution was too weak to give the particle size distribution (data not shown). It should be due to the small size of MFA in MFA/EPO Cryo-GM solution probably less than 1 nm according the detection limit of measurement method. These results also supported the conclusion that MFA/EPO Cryo-GM solution did not contain nanocrystalline MFA.

Solution ^{1}H-T_1 Measurement

^{1}H-T_1 measurement was performed to investigate the molecular mobility of MFA in MFA/EPO Cryo-GM solution. Generally, a longer T_1 means higher mobility, and a shorter T_1 means lower mobility in solution state (44). ^{1}H-T_1 results of MFA dissolved in $CDCl_3$, EPO in acetate buffer, and MFA/EPO Cryo-GM in acetate buffer are shown in Table III. Each ^{1}H-T_1 value for dissolved MFA was determined to be 2.2–2.3 s for aromatic rings and 1.8 s for methyl groups, indicating high molecular mobility. For EPO, low molecular mobility in the solution state resulted in the single and short ^{1}H-T_1 of 0.8 s. In MFA/EPO Cryo-GM solution, the ^{1}H-T_1 of both MFA and EPO changed to approximately 1.0 s, and a single value was obtained. In general, each individual ^{1}H-T_1 in solution-state NMR can provide valuable information on interproton distances and intramolecular motions since they cannot be averaged, unlike the case for solid-state NMR (45). Kalk and Berendsen reported that, at the slow-motion limit (e.g., proteins of molecular weight >10,000 at frequencies exceeding 200 MHz), the T_1 values of individual protons tend to become equal as a result of spin diffusion (45). This supports the idea that MFA of low molecular weight (241.29) differs in its ^{1}H-T_1 by every functional group while high molecular weight EPO (ca. 150,000) indicates an averaged single ^{1}H-T_1. In MFA/EPO Cryo-GM solution, ^{1}H-T_1 values for both aromatic rings and methyl

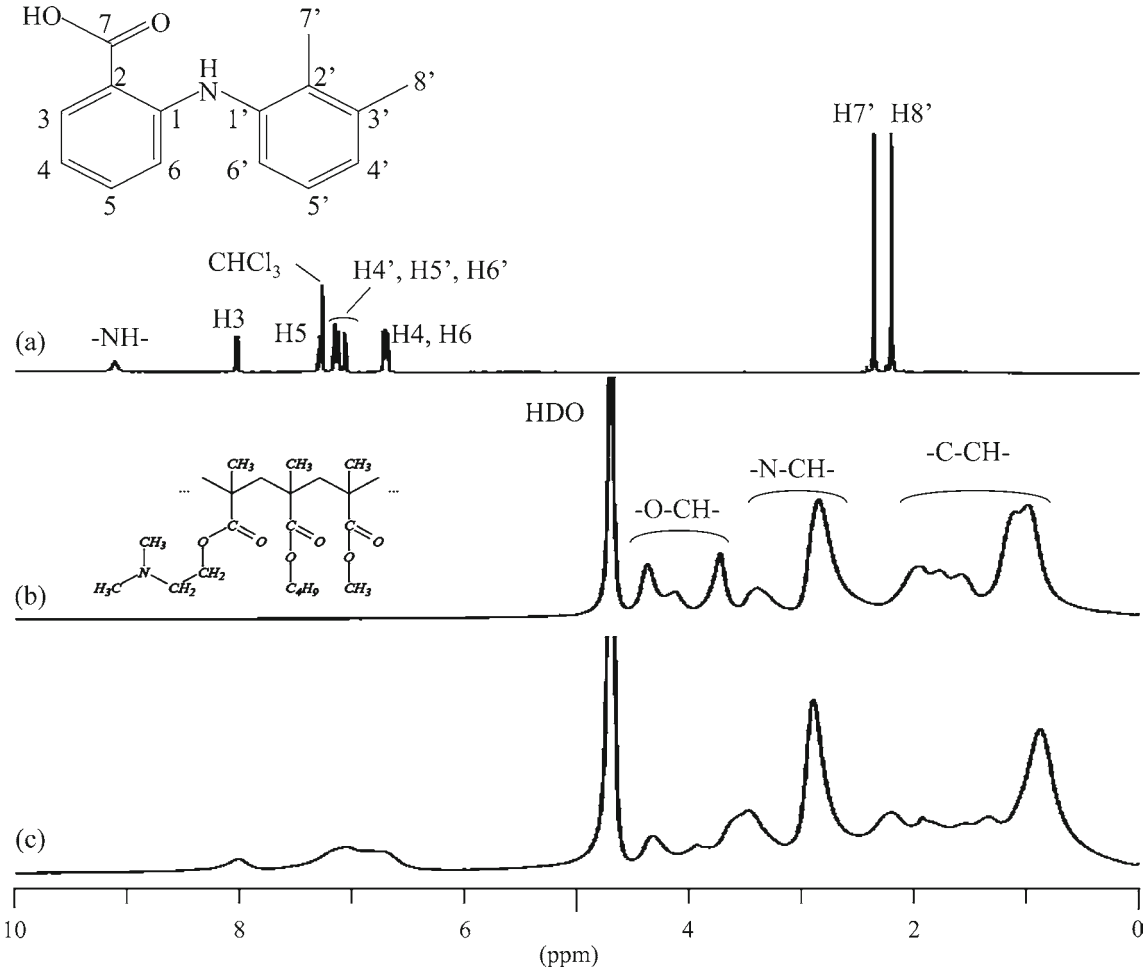

Fig. 7 Solution-state ^{1}H-NMR spectra of (**a**) MFA, (**b**) EPO, and (**c**) MFA/EPO Cryo-GM. MFA was dissolved in $CDCl_3$ while EPO and MFA/EPO Cryo-GM were dissolved in 0.1 M acetate buffer (pH 5.5) prepared from acetic acid-d_4, sodium acetate-d_3, and D_2O.

groups were shortened to the single value of about 1.1 s. It was considered that there was magnetization transfer by cross-relaxation among protons in the MFA molecule (46). Furthermore, the ^{1}H-T_1 of MFA was corresponded to the ^{1}H-T_1 of EPO, also indicating that cross-relaxation occurred between MFA and EPO protons (46). It was speculated that MFA existed as a part of the EPO polymer by forming intermolecular interactions with EPO in MFA/EPO Cryo-GM solution.

Difference NOE Measurement

Direct interaction of MFA with EPO in MFA/EPO Cryo-GM solution was confirmed by the difference NOE experiment. Figure 8 displayed the spectra of MFA/EPO Cryo-GM in acetate buffer at selected irradiation powers for H3 in MFA molecules; irradiation was controlled by changing an attenuator that limited power output. Peak intensity of EPO in the difference spectrum gradually increased according to the increase of irradiation power for H3, and negative NOE correlation was clearly observed. In a difference NOE experiment, longer saturation time led to more magnetization transfer until it reached a steady state (47). Our results strongly support the formation of intermolecular interaction by MFA with EPO in MFA/EPO Cryo-GM solution. We estimated that the inter-nuclear distance between a MFA proton and an EPO proton was less than 0.5 nm since NOE signal is detected between the nuclei within 0.5 nm. It is reported that when the cross relaxation is dominant and a complete saturation of the irradiated spectral component is achieved, a homogeneous negative NOE will be observed throughout the spectrum (45). The single ^{1}H-T_1 of MFA and EPO in Cryo-GM confirmed that spin diffusion could occur in this system. The less specificity of NOE and homogeneous negative NOE throughout the spectrum could be the result that cross relaxation is dominant in the MFA-EPO Cryo-GM. Hence, further precise information about the interacted functional groups and distance was difficult to investigate. From the results of ^{1}H-T_1 measurements in solution, we observed that the ^{1}H-T_1 of MFA in MFA/EPO Cryo-GM in acetate buffer solution became shorter compared with that in $CDCl_3$ solution where

Table III ^{1}H-T_1 of MFA/EPO System in Solution State

^{1}H Assignment (ppm)		T_1 (s)	
		Intact	Cryo-GM
MFA	H3 (8.01)	3.14	1.17
	H5 (7.28)	2.41	1.06
	H6′ (7.15)	2.76	1.06
	H5′ (7.10)	2.73	1.06
	H4′ (7.04)	3.33	1.10
	H6 (6.71)	2.69	1.08
	H4 (6.66)	2.26	1.08
	H7′ (2.33)	1.73	1.15
	H8′ (2.18)	1.82	1.15
EPO	-O-CH-	0.88	1.11
		0.84	1.09
		1.03	1.06
	-N-CH-	0.79	1.11
		0.81	1.02
	-C-CH-	0.87	1.03
		0.84	1.01
		0.85	1.04
		0.87	1.06
		0.84	1.06

MFA alone was monomolecularly dissolved. Decreased T_1 of low molecular weight compounds in the presence of high molecular weight compounds can occur either by intermolecular interaction with the high molecular compound or through increased viscosity of the measuring medium (48). Cross relaxation between MFA and EPO in MFA/EPO Cryo-GM solution clearly confirmed that the decrease in ^{1}H-T_1 of MFA was not the result of increasing viscosity but of formation of intermolecular interaction with EPO.

Effect of Drugs on Supersaturated Behavior of EPO Solid Dispersions

Since MFA and EPO are an acid and a base compounds, the acid–base interaction should be the most possible mechanism for the stabilization of supersaturated solution for a long time. To investigate the structural effect of drugs on the formation of EPO solid dispersion and the subsequent supersaturated behavior, the cryogenic-grinding method was applied to 2 nonsteroidal anti-inflammatory drugs (NSAIDs), IMC and PXC. These compounds contain carbonyl groups that could interact with the aminoalkyl groups of EPO. The drug/polymer ratio was set at 18/82 (w/w). PXRD patterns of IMC/EPO and PXC/EPO systems are shown in Fig. 9. In the patterns of IMC (Fig. 9a), PXC (Fig. 9d), and their PMs (Fig. 9b and e), sharp diffraction peaks derived from their own intact crystalline strucrue were detected, indicating the existence of the crystalline drugs. On the other hand, for both Cryo-GMs with EPO (Fig. 9c and f), all the characteristic diffraction peaks were disappeared and halo patterns were observed. IMC and PXC should transform from crystalline into amorphous states after cryogenic grinding with EPO due to solid dispersion formation.

Figure 10 shows the dissolution profiles of IMC/EPO and PXC/EPO systems in acetate buffer (pH 5.5). Since both IMC and EPO are poorly water-soluble drugs, they reached their low solubility level within 1 h. Slow dissolution of IMC and EPO was also observed in their PMs. In contrast, rapid drug release in the Cryo-GMs with EPO was observed from the beginning of the dissolution test. Within 1 h, all drugs were completely dissolved, and clear supersaturated solutions were obtained. These supersaturated solutions became neither clouded nor precipitated after storage for 1 month at 25°C. Based on these results, we concluded that the formation of a solid dispersion with EPO could enhance the IMC and PXC

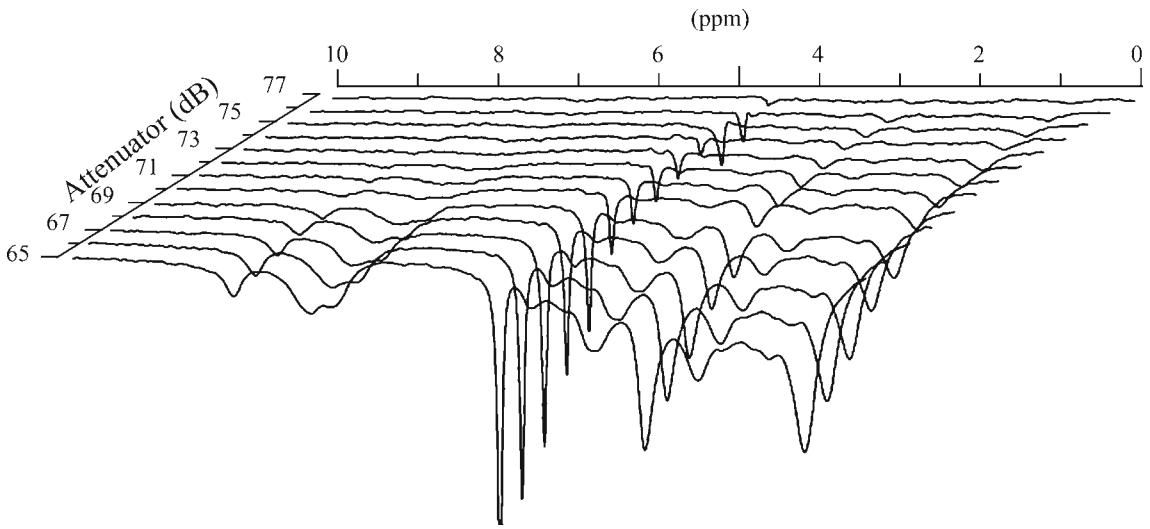

Fig. 8 Difference NOE spectra of MFA/EPO Cryo-GM solution at different irradiation powers.

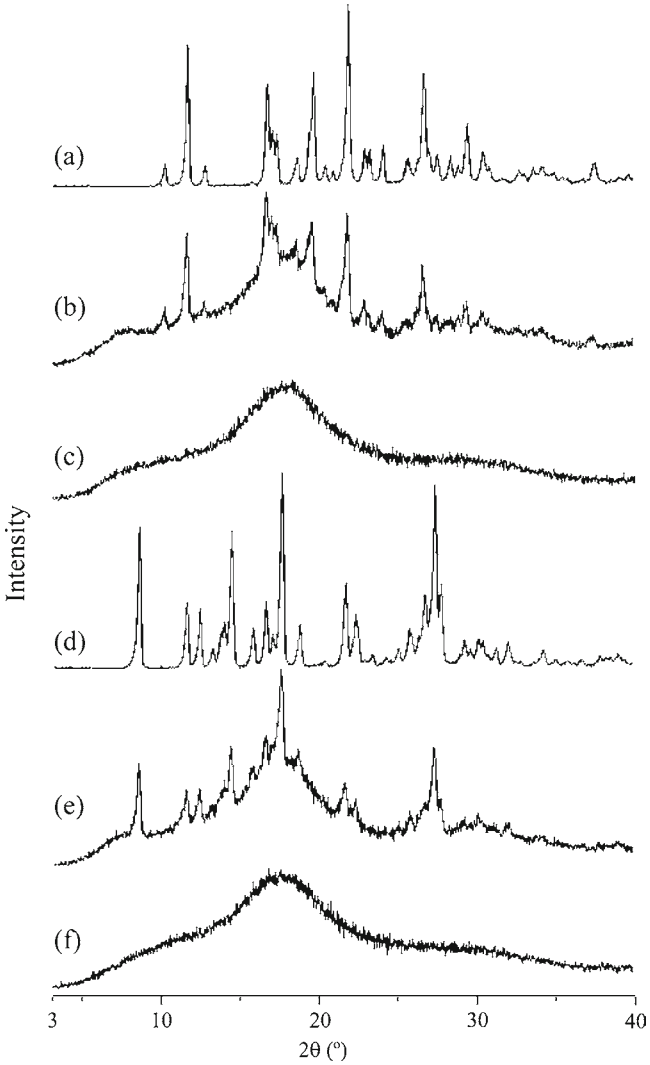

Fig. 9 PXRD patterns of (**a**) IMC, (**b**) IMC/EPO PM, (**c**) IMC/EPO Cryo-GM, (**d**) PXC, (**e**) PXC/EPO PM, and (**f**) PXC/EPO Cryo-GM.

dissolution characteristics significantly. Furthermore, the obtained supersaturated solutions had high stability even after dispersal into acetate buffer solution. Both IMC and PXC, which are acidic drugs, contain carbonyl groups in their structures, similar to MFA. A basic polymer EPO could easily form intermolecular interactions with acidic drugs, and in the present study, the interaction should be mainly formed between the drugs' carbonyl groups and the aminoalkyl group of EPO. Thus, solid dispersions of EPO could be widely used for various drugs, especially acidic drugs, to improve drug solubility and bioavailability.

CONCLUSIONS

Solid dispersion of MFA prepared by cryogenic grinding with EPO showed long-term storage stability in the solid state. A highly supersaturated solution obtained by dispersing the solid dispersion into the buffer solution also exhibited high stability. When the supersaturated solution of MFA was orally administered to rats *in vivo*, an intense increase in bioavailability was observed, indicating the potential usability of EPO solid dispersions for improving the oral absorption of MFA. Solid- and solution-state NMR revealed that MFA and EPO formed interactions with each other at a molecular level. It was indicated that carboxyl group in MFA and aminoalkyl groups in EPO played an important role in the interactions. It was considered that specifically-formed intermolecular interactions between MFA and EPO resulted in the stabilization of the thermodynamically unfavorable monomolecular state in both the solid and solution state. Solubility enhancement by solid dispersion with EPO was also confirmed when IMC and PXC, 2 types of acidic NSAIDs, were used instead of MFA. Solid dispersions with EPO prepared by cryogenic grinding are extremely useful method that can be applied to various kinds of drugs. It should become one of the best answers for the problem concerning about improvement of water solubility and oral bioavailability of poorly water-soluble drugs.

ACKNOWLEDGMENTS & DISCLOSURES

The authors gratefully acknowledge Associate Professor Dr. Hiroko Seki, Dr. Mamoru Imanari, and Dr. Jun Uzawa of the Chemical Analysis Center, Chiba University, for NMR measurement assistance. We would like to thank Evonik

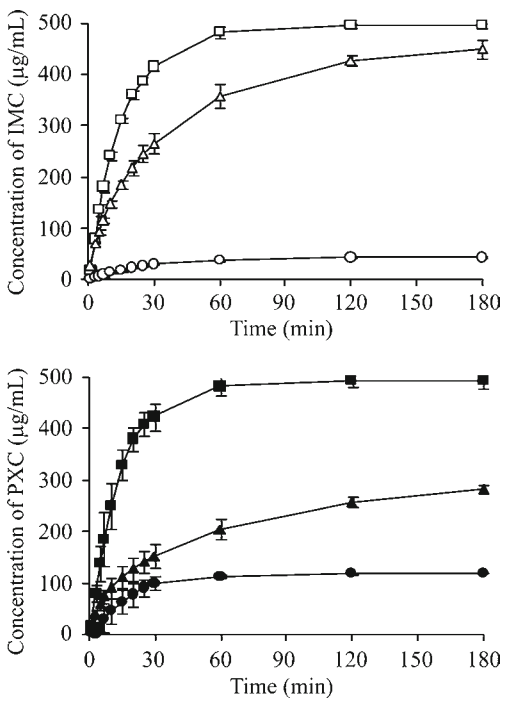

Fig. 10 Dissolution profiles of IMC/EPO (top) and PXC/EPO systems (bottom) at 0.1 M acetate buffer (pH 5.5) (n=3, mean ± SD); (○) IMC, (Δ) IMC/EPO PM, (□) IMC/EPO Cryo-GM, (●) PXC, (▲) PXC/EPO PM, and (■) PXC/EPO Cryo-GM.

Degussa Japan Co. Ltd., for their generous gift of EUDRAGIT®. This study was supported by a Grant-in-Aid for Scientific Research from the Ministry of Education, Culture, Sports, Science and Technology (Monbukagakusho), Japan (21790032, 21590038) and by a Grant from the Japan Health Science Foundation.

REFERENCES

1. Venkatesh S, Lipper RA. Role of the development scientist in compound lead selection and optimization. J Pharm Sci. 2000;89(2):145–54.
2. Yu LX, Amidon GL, Polli JE, Zhao H, Mehta MU, Conner DP, Shah VP, Lesko LJ, Chen ML, Lee VH, Hussain AS. Biopharmaceutics classification system: the scientific basis for biowaiver extensions. Pharm Res. 2002;19(7):921–5.
3. Shiraki K, Takata N, Takano R, Hayashi Y, Terada K. Dissolution improvement and the mechanism of the improvement from cocrystallization of poorly water-soluble compounds. Pharm Res. 2008;25(11):2581–92.
4. Higashi K, Tozuka Y, Moribe K, Yamamoto K. Salicylic acid/gamma-cyclodextrin 2:1 and 4:1 complex formation by sealed-heating method. J Pharm Sci. 2010;99(10):4192–200.
5. Higashi K, Ideura S, Waraya H, Moribe K, Yamamoto K. Incorporation of salicylic acid molecules into the intermolecular spaces of γ-cyclodextrin-polypseudorotaxane. Cryst Growth Des. 2009;9(10):4243–6.
6. Itoh K, Matsui S, Tozuka Y, Oguchi T, Yamamoto K. Improvement of physicochemical properties of N-4472. Part II: characterization of N-4472 microemulsion and the enhanced oral absorption. Int J Pharm. 2002;246(1-2):75–83.
7. Moribe K, Fukino M, Tozuka Y, Higashi K, Yamamoto K. Prednisolone multicomponent nanoparticle preparation by aerosol solvent extraction system. Int J Pharm. 2009;380(1–2):201–5.
8. Wanawongthai C, Pongpeerapat A, Higashi K, Tozuka Y, Moribe K, Yamamoto K. Nanoparticle formation from probucol/PVP/sodium alkyl sulfate co-ground mixture. Int J Pharm. 2009;376(1–2):169–75.
9. Tam JM, McConville JT, Williams 3rd RO, Johnston KP. Amorphous cyclosporin nanodispersions for enhanced pulmonary deposition and dissolution. J Pharm Sci. 2008;97(11):4915–33.
10. Hancock BC, Zografi G. Characteristics and significance of the amorphous state in pharmaceutical systems. J Pharm Sci. 1997;86(1):1–12.
11. Chokshi RJ, Sandhu HK, Iyer RM, Shah NH, Malick AW, Zia H. Characterization of physico-mechanical properties of indomethacin and polymers to assess their suitability for hot-melt extrusion processs as a means to manufacture solid dispersion/solution. J Pharm Sci. 2005;94(11):2463–74.
12. Sivert A, Berard V, Andres C. New binary solid dispersion of indomethacin with surfactant polymer: from physical characterization to *in vitro* dissolution enhancement. J Pharm Sci. 2010;99(3):1399–413.
13. Lakshman JP, Cao Y, Kowalski J, Serajuddin AT. Application of melt extrusion in the development of a physically and chemically stable high-energy amorphous solid dispersion of a poorly water-soluble drug. Mol Pharm. 2008;5(6):994–1002.
14. Friesen DT, Shanker R, Crew M, Smithey DT, Curatolo WJ, Nightingale JA. Hydroxypropyl methylcellulose acetate succinate-based spray-dried dispersions: an overview. Mol Pharm. 2008;5(6):1003–19.
15. Newa M, Bhandari KH, Li DX, Kwon TH, Kim JA, Yoo BK, Woo JS, Lyoo WS, Yong CS, Choi HG. Preparation, characterization and *in vivo* evaluation of ibuprofen binary solid dispersions with poloxamer 188. Int J Pharm. 2007;343(1–2):228–37.
16. Konno H, Handa T, Alonzo DE, Taylor LS. Effect of polymer type on the dissolution profile of amorphous solid dispersions containing felodipine. Eur J Pharm Biopharm. 2008;70(2):493–9.
17. Bothiraja C, Shinde MB, Rajalakshmi S, Pawar AP. Evaluation of molecular pharmaceutical and in-vivo properties of spray-dried isolated andrographolide-PVP. J Pharm Pharmacol. 2009;61(11):1465–72.
18. Vasconcelos T, Sarmento B, Costa P. Solid dispersions as strategy to improve oral bioavailability of poor water soluble drugs. Drug Discovery Today. 2007;12(23–24):1068–75.
19. Quinteros DA, Rigo VR, Kairuz AFJ, Olivera ME, Manzo RH, Allemandi DA. Interaction between a cationic polymethacrylate (Eudragit E100) and anionic drugs. Eur J Pharm Sci. 2008;33(1):72–9.
20. Mollica G, Geppi M, Pignatello R, Veracini CA. Molecular properties of flurbiprofen and its solid dispersions with Eudragit RL100 studied by high- and low-resolution solid-state nuclear magnetic resonance. Pharm Res. 2006;23(9):2129–40.
21. Geppi M, Guccione S, Mollica G, Pignatello R, Veracini CA. Molecular properties of ibuprofen and its solid dispersions with Eudragit RL100 studied by solid-state nuclear magnetic resonance. Pharm Res. 2005;22(9):1544–55.
22. Tishmack PA, Bugay DE, Byrn SR. Solid-state nuclear magnetic resonance spectroscopy–pharmaceutical applications. J Pharm Sci. 2003;92(3):441–74.
23. Pongpeerapat A, Higashi K, Tozuka Y, Moribe K, Yamamoto K. Molecular Interaction among Probucol/PVP/SDS Multicomponent System Investigated by Solid-State NMR. Pharm Res. 2006;23(11):2566–74.
24. Ito A, Watanabe T, Yada S, Hamaura T, Nakagami H, Higashi K, Moribe K, Yamamoto K. Prediction of recrystallization behavior of troglitazone/polyvinylpyrrolidone solid dispersion by solid-state NMR. Int J Pharm. 2010;383(1–2):18–23.
25. Aso Y, Yoshioka S, Zhang J, Zografi G. Effect of water on the molecular mobility of sucrose and poly(vinylpyrrolidone) in a colyophilized formulation as measured by (13)C-NMR relaxation time. Chem Pharm Bull. 2002;50(6):822–6.
26. Schantz S, Hoppu P, Juppo AM. A solid-state NMR study of phase structure, molecular interactions, and mobility in blends of citric acid and paracetamol. J Pharm Sci. 2009;98(5):1862–70.
27. Aso Y, Yoshioka S, Miyazaki T, Kawanishi T, Tanaka K, Kitamura S, Takakura A, Hayashi T, Muranushi N. Miscibility of nifedipine and hydrophilic polymers as measured by 1H-NMR spin– lattice relaxation. Chem Pharm Bull. 2007;55(8):1227–31.
28. Fukuda M, Kitaichi K, Abe F, Fujimoto Y, Takagi K, Takagi K, Morishima T, Hasegawa T. Altered brain penetration of diclofenac and mefenamic acid, but not acetaminophen, in shiga-like toxin II-treated mice. J Pharmacol Sci. 2005;97(4):525–32.
29. Qamar SIN, Ahmad M, Jamshaid M, Muzaffar NA. The bioavailability and pharmacokinetics of mefenamic acid in alloxan-diabetic rabbits. Tokai J Exp Clin Med. 1997;22:163–6.
30. Torchia DA. The measurement of proton-enhanced carbon-13 T1 values by a method which suppresses artifacts. J Magn Reson. (1969). 1978;30(3):613-616.
31. Raghavan SL, Trividic A, Davis AF, Hadgraft J. Crystallization of hydrocortisone acetate: influence of polymers. Int J Pharm. 2001;212(2):213–21.
32. Panchagnula R, Sundaramurthy P, Pillai O, Agrawal S, Raj YA. Solid-state characterization of mefenamic acid. J Pharm Sci. 2004;93(4):1019–29.
33. Gilpin RK, Zhou W. Infrared studies of the thermal conversion of mefenamic acid between polymorphic states. Vib Spectrosc. 2005;37:53–9.
34. Marsac PJ, Li Tonglei, Taylor LS. Estimation of drug-polymer miscibility and solubility in amorphous solid dispersions using

experimentally determined interaction parameters. Pharm Res. 2009;26(1):139–51.
35. McBrierty VJ. N.m.r. of solid polymers: a review. Polymer. 1974;15(8):503–20.
36. McBrierty VJ, Douglass DC. Recent advances in the NMR of solid polymers. J Polym Sci Macromol Sci Rev. 1981;16(1):295–366.
37. Calucci L, Galleschi L, Geppi M, Mollica G. Structure and dynamics of flour by solid state NMR: effects of hydration and wheat aging. Biomacromol. 2004;5(4):1536–44.
38. Dokorou V, Ciunik Z, Russo U, Kovala-Demertzi D. Synthesis, crystal structures and spectroscopic studies of diorganotin derivatives with mefenamic acid. Crystal and molecular structures of 1,2:3,4-di-[mu]2-2-[(2,3-dimethylphenyl)amino]-benzoato-O,O-1,3-bis-2-[(-[(2,3-dimethylphenyl)amino]benzoato-O-1,2,4:2,3,4-di-[mu]3-oxo-tetrakis[di-methyltin(IV)] and 1,2:3,4-di-[mu]2-2-[(-[(-[(2,3-dimethylphenyl)amino]-benzoato-O,O-1,3-bis-2-[(-[(-[(2,3-dimethylphenyl)amino]benzoato-O-1,2,4:2,3,4-di-[mu]3-oxo-tetrakis[di-n-butyltin(IV)]. J Organomet Chem. 2001;630(2):205–14.
39. Separovic F, Chau HD, Burgar MI. Solid-state NMR study of aging of Colorbond polymer coating. Polymer. 2001;42(3):925–30.
40. Lim AR, Kim JH, Novak BM. Solid state 13C nuclear magnetic resonance for polyguanidines. Polymer. 2000;41(7):2431–8.
41. Luo H, Chen Q, Yang G, Xu D. Phase structure of ethylene-dimethylaminoethyl methacrylate copolymers and its relation to comonomer content as studied by solid-state high-resolution ^{13}C n.m.r. spectroscopy. Polymer. 1998;39(12):943–7.
42. Aso Y, Yoshioka S. Molecular mobility of nifedipine–PVP and phenobarbital–PVP solid dispersions as measured by 13C-NMR spin-lattice relaxation time. J Pharm Sci. 2006;95(2):318–25.
43. Heald CR, Stolnik S, Kujawinski KS, De Matteis C, Garnett MC, Illum L, Davis SS, Purkiss SC, Barlow RJ, Gellert PR. Poly(lactic acid)−Poly(ethylene oxide) (PLA−PEG) Nanoparticles: NMR Studies of the Central Solidlike PLA Core and the Liquid PEG Corona. Langmuir. 2002;18(9):3669–75.
44. Breitmaier E, Voelter W. Carbon-13 NMR spectroscopy: high resolution methods and applications in organic chemistry and biochemistry. Verlag Chemie: Weinheim; 1986.
45. Kalk A, Berendsen HJC. Proton magnetic relaxation and spin diffusion in proteins. J Magn Reson. 1976;24(3):343–66.
46. Bhowmik A, Ellena JF, Bryant RG, Cafiso DS. Spin-diffusion couples proton relaxation rates for proteins in exchange with a membrane interface. J Magn Reson. 2008;194(2):283–8.
47. Bondarenko V, Yushmanov VE, Xu Y, Tang P. NMR study of general anesthetic interaction with nAChR beta2 subunit. Biophys J. 2008;94(5):1681–8.
48. Martini S, Consumi M, Bonechi C, Rossi C, Magnani A. Fibrinogen −catecholamine interaction as observed by NMR and fourier transform infrared spectroscopy. Biomacromolecules. 2007;8(9):2689–96.